

# Gravitational Wave emission in Binary Neutron Star early post-merger within a dark environment

D. Suárez-Fontanella,<sup>\*</sup> D. Barba-González,<sup>†</sup> C. Albertus,<sup>‡</sup> and M. Ángeles Pérez-García<sup>§</sup>  
*Department of Fundamental Physics and IUFFyM, University of Salamanca,*  
*Plaza de la Merced S/N E-37008, Salamanca, Spain*

(Dated: August 13, 2024)

Using an effective Lagrangian model inspired by [1] we describe the early post-merger of a binary Neutron Star (BNS) merger event with a non-vanishing ambient fraction of dark matter. For this we mimic the dynamics of two oscillating Neutron Star (NS) masses in the gravitational potential well as they merge. We parametrize the ejected baryonic matter fraction in the coalescence event forming a surrounding debris disk containing a non-vanishing dark matter fraction. In order to analyze the dark contribution, we start from a dark-matter free modelization using Monte Carlo Markov Chain (MCMC) techniques to replicate the gravitational waveforms obtained from simulations in the CoRe database for three selected equations of state for NS matter (DD2, BHBlp, SFHo). Later, we explore the impact of a dark viscous fluid under a prescribed velocity dependent force and obtain the waveforms and spectral properties originating in the first few ms in the BNS post-merger. Finally we discuss our findings in light of the prospects of detectability of a non-vanishing fraction of dark matter arising in the waveforms and power spectral distribution in present or future experimental settings.

## I. INTRODUCTION

The detection of dark matter (DM) is one of the most exciting and enigmatic current challenges in astrophysics, cosmology and particle physics. On-going searches of this elusive type of matter include different strategies. Namely they are mostly associated to scattering events (direct searches), production of secondaries such as photons or neutrinos (indirect searches) or production in hadron colliders and beam-dump experiments at high energies (collider searches), see [2] for a review. There is now a vast literature on the phenomenology associated to the, otherwise, feebly interacting dark sector [3]. Current models predict that based on prescribed interactions with ordinary matter, up to  $\sim 10\%$  mass fraction can reside as DM in the Neutron Star (NS) stellar volume [4] and beyond. Halo distributions where radial extent of DM is beyond the baryonic value,  $R_\chi > R_b$ , are also possible for light and weakly bound DM candidates [5].

So far different particle candidates have been proposed to account for the DM. Ranging from weakly to strongly interacting species and for a mass range spanning many orders of magnitude, there are plenty of models in the literature. Just to cite a few of them, let us remind here the weakly interacting massive particle (WIMP) such as the supersymmetric neutralino, asymmetric dark matter (ADM), light bosons such as axions or axion-like particles and strangelets [6]. Although much theoretical and experimental efforts have been undertaken, its nature remains elusive, constituting an open problem. Nevertheless, there is now overwhelming evidence of its existence

more than nine decades after the pioneering observations by Fritz Zwicky in 1933 [7], who showed that the velocities of galaxies in the Coma cluster greatly exceeded the expectations based solely on the sum of the individual luminous galaxy masses. Since then, wide searches involving different strategies trying to hunt these exotic particles have shown null results although the phase space is now more tightly constrained.

Remarkably, the dawn of the era of multimessenger physics allows to gather information on different channels enriching the picture and more efficiently constraining the physical mechanisms governing its behaviour. In particular, gravitational waves (GWs) experiments are expected to provide a precise reconstruction of the properties of inspiraling and merging compact objects, including mass/radius/composition measurements as they would be sensitive to tiny deviations in the gravitational waveforms which may be induced by matter features in the violent events of the merging black holes (BHs) and NSs. These environmental effects could be the smoking-gun to signal the presence of DM, although this requires a careful identification of the ordinary baryon content [8].

Since the LIGO first detection in 2015 of GWs emitted during the merger of a stellar-mass binary black hole (BBH) merger event [9], the possibility to add this new multimessenger opens a new window to the Universe. In addition, GWs provide a new channel to shed light on the nature of DM, also constituting a definite confirmation that BBHs exist and merge with a local rate [10] in the range between  $17.9$  and  $44 \text{ Gpc}^{-3} \text{ yr}^{-1}$  at a fiducial redshift ( $z = 0.2$ ), assuming the known sources are representative of the total population. Other compact binary coalescence (CBC) search targets include collisions of BHs and NSs or a binary NS merger (BNS), where in all of them GWs are produced in a transient emission that can be detected on current terrestrial facilities. Recently, detectors including LIGO-Virgo-Kagra

<sup>\*</sup> duvier@usal.es

<sup>†</sup> david.barbag@usal.es

<sup>‡</sup> albertus@usal.es

<sup>§</sup> mperezga@usal.es

(LVK) have released enough data to build catalogs currently listing nearly 100 detections [11]. Specifically the Gravitational-Wave Transient Catalog 3 (GWTC-3) [10] contains signals consistent with three classes of binary mergers. They infer the BNS merger rate to be between 10 and 1700  $\text{Gpc}^{-3}\text{yr}^{-1}$  and the NS-BH merger rate to be between 7.8 and 140  $\text{Gpc}^{-3}\text{yr}^{-1}$ , assuming a constant rate density in the comoving frame and taking the union of 90% credible intervals. Besides these efforts, other future 3rd-generation planned detectors such as Cosmic Explorer (CE) [12], Einstein Telescope [13], NEMO[14] or LISA[15] will be able to further detect ultralow and ultraweak GW spectral sensitivities of the order  $h \sim 10^{-25} \text{Hz}^{-1/2}$  produced by massive cosmic events with redshifts  $z \lesssim 10$  and total mass around that expected in BNS  $M \lesssim 3M_{\odot}$ .

Very recently an intriguing event, GW230529 [16], was observed during the fourth observing run of the LVK detector network on 2023 May 29 by the LIGO Livingston Observatory. Its estimated primary mass was about  $3.6M_{\odot}$ . GW230529 is the first binary candidate with the primary component in the mass gap, i.e. being a BH of mass smaller than  $5M_{\odot}$ . However, the probability that the primary component is a NS is small but non-zero. On the other hand, the secondary component of GW230529, the mass of which has a 90% chance of lying between  $[1.2, 2.0]M_{\odot}$  is almost certainly a NS.

In this work we will use a Lagrangian effective model inspired by [1, 17] tailored to study the dynamics of the early post-merger phase in a BNS merger occurring in an environment polluted by viscous DM. Thus in our model the BNS environment possesses a baryonic mass fraction  $f_b$  and DM fraction  $f_{\chi}$  during the GW emission. In this way we are able to compute the set of polarization strengths  $h_{+, \times}(t)$  of the GW signal as a function of time  $t$  and subsequent observables derived from them. We note that, at present, there are additional tools such as Bilby [18], a Bayesian inference library for gravitational-wave astronomy, allowing to infer the source astrophysical properties from existing experimental data. This tool does not incorporate, however, particular realizations of exotic models including DM like the one we present in this work.

In our setting the presence of DM in the system is due to the actual BNS merger having place in a DM polluted environment. It may be due to stripped DM from the inside of the NS or from an overdensity or halo where typically DM density can be much larger with respect to the solar neighbourhood value  $\rho_{\chi} \simeq 0.4 \text{ GeV}/\text{cm}^3$ . It has been recently claimed [19] that even overdensities of a few  $\sim 10^4 \text{ GeV}/\text{cm}^3$  at 1 parsec from the center of M4 would not yield definite constraints on DM from kinetically heating of NSs or white dwarfs.

The detection of DM using GW along with different strategies has already been discussed, see [8]. One of the key ideas is based on the fact that it constitutes a fingerprint of the formation and evolution of first cosmic structures. Popular models include cold DM (CDM) on sub-galactic scales. However, there still remain incom-

patibilities between the CDM description and the observed data, as it predicts more structure on small scales than what we actually observe. Other models such as warm or fuzzy DM, as shown by simulations, lead to the suppression of small-scale structures and this, in turn, may lead to a significant reduction in the rate of BBH mergers observed, helping to further constrain among existing DM models. On the small scales, collisionless DM fluid faces major issues such as the core cusp problem, missing satellites problem, too big to fail problem. For more detail on the small scale issues, see [20]. This shows that future GW observations will provide a new probe of physics beyond the  $\Lambda$ CDM model [21].

The possible traces that many of the DM candidates could leave on the patterns of GW polarizations has been a particularly effervescent topic in the last decade [22–26]. The existence of viscous and self-interacting DM (SIDM) is another key point. At the small scale, the SIDM behaves like a collisional dark matter but on the large scale it behaves like the collisionless DM, thus fitting expectations. In [27] it is pointed out that the collisional nature of DM can lead to viscosity and using the kinetic theory and viscous coefficients of the SIDM can be obtained. Therefore the ratio of the SIDM cross section to its mass ( $\sigma/m_{\chi}$ ), for the present observed cosmic acceleration, can be reconciled with the constraints obtained from astrophysical observations. Note that a GW will also experience the damping effect when it propagates in a fluid with non-zero viscosity so that the constraints of the luminosity distances from the observed GW events by experiments can be directly used to set constraints on self-interactions [28, 29].

The structure of this contribution is as follows. In section II the Lagrangian model is introduced along with the relevant set of parameters necessary to describe the GW polarizations and subsequent quantities obtained from them. In our description, inspired by the mechanics of a two-body oscillator, we include typical BNS merger associated quantities, such as the mass ratio and the chirp mass, aimed to effectively describe the GW emission. We discuss how the presence of a hybrid viscous medium allows mimicking selected GW catalog waveforms during the  $\sim 3 \text{ ms}$  timescale after the merger. Thus we will compare signals from recent numerical relativity simulations from the Computational Relativity (CoRe) database [30] involving several equations of state (EoS). In section II A, the different polarization modes in the GW from the selected dataset are fit, first to a DM-free model, in order to assess the efficiency of the Monte Carlo Markov Chain (MCMC) based fitting procedure allowing for a parameter estimation and, later on, allowing for a non-vanishing viscous DM fraction. We provide a physical insight of the effective parameters used.

In section III we calculate the power spectral density (PSD) in order to characterize the frequency domain of the expected GW features and the sensitivity of current and future detectors to novel dark components, based on the relative effective signal-to-noise ratio for differ-

ent DM polluted environments. Finally in section IV we conclude.

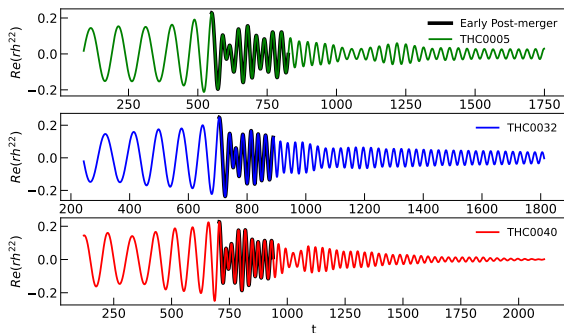


FIG. 1: Principal mode  $h^{22}$  data as a function of time from three simulations (THC0005, THC0032, THC0040) from CoRe database [30] obtained using WhiskyTHC. Our fitting dataset is limited to the early post-merger stage (highlighted in dark in each waveform). Time axis is expressed in  $GM_{\odot}/c^3 \simeq 4.92549 \times 10^{-6}$  s units.

## II. MODEL FOR THE EMISSION OF GRAVITATIONAL WAVES

First we will introduce the Lagrangian model that we will use in order to calculate the GW emission in the post-merger phase of the BNS event. The system we will scrutinize are the first few ms right after the NSs merge. Note that in this phase, strong tidal forces have already disrupted the otherwise nearly spherical (rotating) stellar configuration in asymptotically early times before the merger. In our scenario we will assume that a dark polluted environment is present due to a non-vanishing fraction of DM coexisting with the expected baryonic matter mass fraction expelled in the collision. This dark fraction origin may well come either from a liberated dark population loosely bound in superficial stellar layers or beyond baryonic radii, such as in halo configurations, see [4] or from an existing local DM overdensity if the BNS merger takes place inside a DM cluster.

As computational simulations show [31], for the few ms duration the BNS early post-merger dynamics can be mimicked by that of a damped oscillator (DO). This notion arises naturally as the GW transient emission takes place in a baryon environment with associated dissipative oscillating dynamics from ordinary (nuclear) matter.

In this scenario, we study how a fluid composed of massive  $\chi$  particles may leave a fingerprint in the transient emission of the BNS merger event we model, using a minimally coupled DM model. In this respect DM should be thermalized with the NS stellar matter so that it can (at least partially) follow the dynamics of the merger. This condition is fulfilled for DM models yielding constant

scattering spin-independent  $\chi$ -nucleon cross-sections for  $m_{\chi} \gtrsim 1$  GeV/ $c^2$ ,  $\sigma_{\chi,N} \gtrsim 10^{-45}$  cm<sup>2</sup>, see [32]. Further couplings at the strong (hadronic) force limit are theoretically possible yielding a more ultradense environment [33] driving the final object to a BH collapse. However, we will restrict the DM sector we consider to yet another fraction of matter component, essentially inert with respect to changes in ordinary baryonic matter species. Thus in the post-merger the stellar configuration corresponds to that of two stellar nucleus surrounded by a disk (assuming some composition of previous spin from the merging stars) with baryonic and DM content. The actual proportions of the total mass in the disk and nuclei are to be determined dynamically, see below.

### A. Binary Neutron Star merger as a damped oscillator

As mentioned, we describe this early post-merger as a DO immersed in ejecta material. For simplicity we will use a viscous (dissipative) force  $F_{b,d} \sim v_r^n$  as a power of radial velocity  $v_r = \dot{r}$ . We will consider that the DO dynamics are affected by this non-ideal behavior in two ways, first from a nuclear (baryon) fluid with associated quadratic viscous resistance  $F_{b,d} \sim -\alpha_2 \dot{r}^2$  while a less dense, diffuse DM fraction contributes instead  $F_{\chi,d} \sim -\beta_n \dot{r}^n$ .  $\alpha_2, \beta_n$  ( $n = 1, 2$ ) are effective parameters characterizing both types of matter that will be discussed later.

Using MCMC we will fit the oscillation modes as a function of time, obtained from simulations such as CoRe database [30] for a set of three different EoS, namely BHB1p [34], SFHo [35], and DD2 [36]. All of them can describe NS matter with a non-zero viscosity and finite temperature. As described in [31, 37], immediately after the merger, peak temperatures  $T \sim 80$  MeV are reached. We note the dark fluid we introduce will nevertheless be a small mass fraction with a proper viscosity that may be lower or comparable to that of baryons. As discussed, the ultimate source of DM viscosity is an assimilated non-zero self-interaction or  $\chi$ -nucleon cross-section that although weak in strength may be, however, similar to photon-photon scattering in electromagnetic plasmas for energies or hundredths of MeV.

More specifically dark and baryonic matter will be expelled from the NS outer layers, less gravitationally bound, due to the tidal forces. In our setting we will consider this fraction of ejected matter forms a disk around the NS nuclei rotating with the same angular velocity. Note that this picture is what current numerical relativity simulations yield [38] and the scenario for kilonova emission, detectable with Earth based telescopes such as MAAT [39], in the neutron-rich environment formed after the merger.

We implement this scenario by means of two merging NSs with gravitational masses  $m_1$  and  $m_2$  in a rotating disk with a fraction of DM,  $f_{\chi}$ , and an ordinary i.e. bary-

onic fraction,  $f_b$ , whose origin is the debris of the tidal disruption of the two compact stars. In the mechanical analog, both spheres are connected by a spring characterized by constant  $k$ . The spheres can oscillate along the radial coordinate and rotate on the two-dimensional orbiting plane. For the sake of simplicity, we will consider an observer perpendicular to the plane where the orbital motion happens. As the damping oscillation proceeds, there will be a dynamical variation of the moment of inertia of the system and, from the conservation of angular momentum, this will be resulting in the generation of GW with a specific spectrum.

This model is inspired by previous works [1, 17] describing, however, a different case i.e. a four-mass oscillator where two DM and two NS matter cores oscillate jointly with two different springs with constants  $k_1, k_2 \neq k_1$ . Our model is different as it considers the fact that the oscillations happen in a dark environment and aims at exploring the spectral features observed in the early post-merger signal. As we will describe, the frequencies and amplitudes of these oscillations will be affected by the presence of DM and this, in turn, determines the spectral properties of the GW signal.

Despite its simplicity, this effective model can reproduce the complex waveforms emitted in the early BNS merger and provide insights into the physical interpretation of the various peaks in the spectrum. It provides a convenient tool to improve post-merger signal description and modeling, potentially enabling the development of comprehensive analytical models for template construction including a DM component.

In order to evaluate the sensitivity of our model to DM in the predicted GW signal strength we will keep restricted to a minimum the number of extra parameters describing the dark environment where the BNS happens. As we will explain, we include namely the DM mass fraction  $f_\chi$  and one physical parameter, a dissipative coefficient,  $\beta_n$ , describing the radial velocity ( $\dot{r}$ ) dependent viscous force  $F_{\chi,d} \sim \beta_n v^n$ , characterizing the presumable viscosity of the low-density DM fluid. Note that this effectively non-relativistic parametrization is based on the fact that there may be non-vanishing cross-sections among the two sectors and a possibly self-interacting term in the dark sector. As we will show, the non-relativistic nature of DM dynamics can be included in our minimal scenario in a meaningful way, yielding characteristic features capable of constraining some DM models.

As mentioned above, the Lagrangian we consider is able to reproduce not only the GW polarizations but also many spectral properties of the BNS early post-merger signal. Thus the BNS merger event can be thought of in this scenario as two phases. In a first phase of the merger the outer NS layers are stripped off due to the tidal fields, carrying away the baryonic mass  $m_b = f_{\text{ejec}}(m_1 + m_2) \equiv f_{\text{ejec}}M_T$  from the progenitor stars ( $m_1, m_2$ ) rapidly forming a disk-like structure

with a radius  $R_d$ , enclosing the two NS inner nuclei of masses  $(1 - f_{\text{ejec}})m_1$  and  $(1 - f_{\text{ejec}})m_2$ , respectively bound by an elastic force of constant  $k$ . We use equivalently  $f_{\text{ejec}} \equiv f_b$ . The minimum elongation happens at a characteristic radial distance,  $l$ , from the coordinate origin. The original motivation of this oscillating behaviour is guided by numerical relativity simulations showing this effect in a gravitational potential well created during the merger phase [40]. Thus we will be assuming that the existence of this elastic force is an approximation that captures the behavior of these two NS nuclei and their motion in a quasi-elliptical orbit.

Due to the abrupt fall of the tidal field after the disruption of the outer layers and the conservation of angular momentum, these nuclei keep rotating inside this pre-collapsed object with the same angular velocity  $\omega \equiv \dot{\theta}$ , which therefore has a metastable nature. Later on, a complete fusion is occurring inside (second phase) as soon as the rotational energy of these nuclei decays due to dissipation through interactions with the surrounding matter in the radial direction.

For now, focusing on the interest of this work, we will restrict ourselves to the first of these phases, during which a fraction  $f_\chi = m_\chi/M_T$  of DM is present in the disk from the environment. Both  $f_b, f_\chi$  are small fractions at the per-cent level, as numerical relativity simulations seem to indicate [38, 41]. We set the origin of coordinates at the center of mass of the merging NSs and use as dynamical variables the distance from the center of coordinates to one of the spheres and its angle ( $r, \theta$ ) to describe the two degrees of freedom of the system.

For a system of mass ratio  $q = m_1/m_2$ , we can write the following Lagrangian as *ideal* starting point

$$\mathcal{L} = (1 - f_{\text{ejec}})q \frac{M_T}{2} (\dot{r}^2 + (r\dot{\theta})^2) + (f_{\text{ejec}} + f_\chi) \frac{M_T}{2} R_d^2 \dot{\theta}^2 - \frac{k}{2} (1 + q^2) \left( r - \frac{l}{1 + q} \right)^2. \quad (1)$$

Note that the chirp mass may also be used as it is straightforwardly related to the total mass as

$$\mathcal{M}_c = \left[ \frac{q}{(1 + q)^2} \right]^{3/5} M_T, \quad (2)$$

and quite precisely measured in BNS mergers.

We now proceed to generalize the previous idealized oscillator by considering damping may be present due to dissipation. This is physically motivated by the prediction of finite values of NS matter microscopic viscosities for numerous EoS. This has been thoroughly studied in the literature [42, 43]. Models for DM may also include a viscous character by construction, as discussed in Section I.

For the sake of concreteness we will consider that for the strongly interacting NS matter the dissipative force in the Lagrangian dynamics can be generically described

as a radial force proportional to  $n$ -power of radial velocity  $v_r^n = \dot{r}^n$  with a density-dependent coefficient,  $\alpha_n$ , proportional to the linear density of ejected matter.

$$F_{b,d} = -f_{\text{ejec}} \frac{M_T}{R_d} (\alpha_1 \dot{r} + \alpha_2 \dot{r}^2), \quad (3)$$

where  $\alpha_1, \alpha_2$  are the effective dissipative coefficients of baryonic matter. Similarly, for the dark sector we will consider the possibility of so-called Coulomb damping and viscous damping, both  $v_r$ -dependent with coefficients  $\beta_n$

$$F_{\chi,d} = -\frac{m_\chi}{R_d} (\beta_1 \dot{r} + \beta_2 \dot{r}^2) = -f_\chi \frac{M_T}{R_d} (\beta_1 \dot{r} + \beta_2 \dot{r}^2). \quad (4)$$

Due to the different nature of both sectors and combining the baryonic and DM contributions we will set the effective dissipative force as

$$F_d = -\alpha_2 \frac{m_b}{R_d} \dot{r}^2 - \beta_1 \frac{m_\chi}{R_d} \dot{r} - \beta_2 \frac{m_\chi}{R_d} \dot{r}^2, \quad (5)$$

setting  $\alpha_1 \equiv 0$ , or expressed in terms of mass fractions as

$$F_d = -[f_{\text{ejec}} \alpha_2 \dot{r}^2 + f_\chi (\beta_1 \dot{r} + \beta_2 \dot{r}^2)] \frac{M_T}{R_d}. \quad (6)$$

We can now apply the Euler-Lagrange formalism to obtain the equations of motion for spatial coordinates  $(r, \theta)$  under the form

$$d_t \partial_{\dot{r}} L - \partial_r L = \partial_r F_d \quad (7)$$

$$d_t \partial_{\dot{\theta}} L - \partial_\theta L = \partial_\theta F_d. \quad (8)$$

with  $d_t \equiv \frac{d}{dt}$  the time derivative operator. Note that for the dissipative terms,  $F_d$ , the only non-vanishing contribution results from the radial velocity dependence.

$$\partial_r F_d = -(2f_{\text{ejec}} \alpha_2 \dot{r} + \beta_1 f_\chi + 2f_\chi \beta_2 \dot{r}) \frac{M_T}{R_d}. \quad (9)$$

Finally the equations of motion read

$$\begin{aligned} \ddot{r} + \frac{(\alpha_2 f_{\text{ejec}} + \beta_2 f_\chi)}{(1 - f_{\text{ejec}})} \frac{2}{q R_d} \dot{r} - \dot{\theta}^2 r + \\ \frac{(1 + q^2)}{(1 - f_{\text{ejec}})} \frac{k}{\xi} \left( r - \frac{l}{1 + q} \right) + \beta_1 \frac{f_\chi}{(1 - f_{\text{ejec}})} \frac{1}{q R_d} = 0, \\ (r^2 + \frac{f_{\text{ejec}} + f_\chi}{1 - f_{\text{ejec}}} \frac{R_d^2}{q}) \ddot{\theta} + 2r \dot{r} \dot{\theta} = 0, \end{aligned} \quad (10)$$

where  $\xi \equiv q M_T$ .

### 1. GW Polarizations

To compute the GW polarizations,  $h_\times, h_+$  we employ the time variation of the reduced quadrupole moment

$Q_{ij} = I_{ij} - \frac{1}{3} \delta_{ij} \delta^{\mu\nu} I_{\mu\nu}$  with  $i, j = 1, 2, 3$  in Cartesian coordinates.  $I_{ij}, \delta_{ij}$  are the moment or inertia and Kronecker delta, respectively. With these definitions, we can write [1, 44]:

$$h_+ = \frac{\ddot{Q}_{11} - \ddot{Q}_{22}}{d}, \quad h_\times = \frac{2\ddot{Q}_{12}}{d} \quad (11)$$

where  $d$  represents the distance to an optimally oriented i.e face-on observer. Using that

$$I_{ij} = \frac{M_T}{2} r^2 \tilde{I}_{ij}, \quad (12)$$

where  $\tilde{I}_{ij}$  is

$$\begin{pmatrix} 1 + \cos(2\theta) & \sin(2\theta) \\ \sin(2\theta) & 1 - \cos(2\theta) \end{pmatrix}, \quad (13)$$

and since  $Q_{11} = \frac{M_T}{2} r^2 (\frac{1}{3} + \cos(2\theta))$ ,  $Q_{22} = \frac{M_T}{2} r^2 (\frac{1}{3} - \cos(2\theta))$  and  $Q_{12} = \frac{M_T}{2} r^2 \sin(2\theta)$  it finally results

$$h_+ d = A(r, \theta) \cos(2\theta) - B(r, \theta) \sin(2\theta), \quad (14)$$

$$h_\times d = B(r, \theta) \cos(2\theta) + A(r, \theta) \sin(2\theta). \quad (15)$$

Functions  $A(r, \theta)$  and  $B(r, \theta)$  can be obtained from the Lagrangian in Eq. (1) as

$$A(r, \theta) = 2(1 - f_{\text{ejec}}) q M_T (\dot{r}^2 + r \ddot{r} - 2r^2 \dot{\theta}^2) \quad (16)$$

$$B(r, \theta) = 2(1 - f_{\text{ejec}}) q M_T (4r \dot{r} \dot{\theta} + r^2 \ddot{\theta}) \quad (17)$$

Note that the ambient DM present during the merger is characterized by a non-vanishing fraction  $f_\chi \neq 0$ , although we will consider cases where it has either viscous or inviscid nature. This is the minimal assumption that we have introduced as we aim to probe its potential implications on the polarization shape of the waves and spectral properties. More in-depth DM characterization would involve a non-trivial mixing among the two sectors that we will leave for a future work.

To elucidate these effects, we will proceed as follows. First, we will calibrate the DM-free model by obtaining a parameter set adjusting waveforms in the early BNS post-merger from existing numerical relativity simulations. Later on, we will allow a non-zero set of  $f_\chi, \beta_{1,2}$  in order to determine the impact on the results. We will be considering three pivotal scenarios. One where DM exhibits no viscosity ( $f_\chi \neq 0, \beta_1 = \beta_2 = 0$ ), a second one where it showcases viscosity, albeit lower by a factor  $\sim 1/10$  than for baryonic matter sourced from stars ( $f_\chi \neq 0, \beta_{1,2} < \alpha_2$ ), and lastly, a scenario where viscosity is similar or larger as compared to baryonic matter ( $f_\chi \neq 0, \beta_2 \gtrsim \alpha_2$ ). To accomplish these tasks, we will employ fitting methodologies grounded in Monte Carlo methods implemented in Python language, see below.

## 2. Fitting data sets

For our study, we use the CoRe database [30] of BNS simulations restricted to a few ms in the early post-merger. The region of interest to our calculation is depicted in Fig.(1) highlighted with a dark line for each waveform. Time axis is expressed in  $GM_\odot/c^3 \simeq 4.92549 \times 10^{-6}$  s units. From top to bottom we plot the principal mode data  $h^{22}$  from three simulations in the catalog (THC0005, THC0032, THC0040) obtained using WhiskyTHC [45].

Specifically, we extracted simulation data from THC005, THC0032, and THC0040, employing the set of BHB1p [34], SFHo [35], and DD2 [36] EoS, respectively, incorporating nuclear viscosity. The selected dataset shows some spread regarding initial BNS configurations. For example, THC0005 Fig.(1) top panel, relates to a BNS simulation with progenitor masses  $m_1 = 1.2M_\odot$  and  $m_2 = 1.4M_\odot$ . Stellar structure equations associate for the BHB1p EoS their approximate radii as  $R_{1,2} \approx 13.0$  km [34]. THC0032 in Fig.(1) middle panel accurately reproduces the GW signature generated by two NSs with masses  $m_1 = 1.20M_\odot, m_2 = 1.40M_\odot$ , corresponding to approximate radii of  $R_1 = R_2 = 11.50$  km. Similarly, for THC0040 Fig.(1) lower panel, NS masses are  $M_1 = 1.30M_\odot, M_2 = 1.43M_\odot$  with radii  $R_1 = R_2 = 13.0$  km. In our setup we fix somewhat arbitrarily an approximate disk radius  $R_d \simeq 15.44$  km.

From simple inspection, we see additional information regarding this GW mode, summarized in the shapes depicted in Fig.(1). We will analyze it further in the framework of the full model when the DM component is incorporated, see below. The quoted values of mass and radius from study cases in simulations will serve as initial sampling points within the parameter space of our model.

In the model presented, the parameter space encompasses the 10-tuple  $(k, \alpha_2, \omega_0, r_0, l, \tilde{f}, m_1, m_2, f_\chi, \beta_n)$  selecting  $n = 1, 2$  or  $\beta_n \equiv 0$  and  $\omega(t_{\text{merger}}) \equiv \omega_0, r(0) \equiv r_0$ . Each parameter holds a distinct physical significance. Specifically,  $k$  is the effective spring constant of the elastic force in the oscillator-like gravitational potential in the post-merger.  $\alpha_2, \beta_n$  represent the linear density dependence associated with quadratic (or n-power) dissipative forces in Eq. (5) for the ordinary (dark) sector.  $\omega_0$  is the initial angular velocity of the system, intricately linked to that of the binary system at the moment of merger.  $r_0$  stands for the initial separation distance between the cores, while the parameter  $l$  represents the length where the elastic force between the cores reaches its minimum value. The parameter  $\tilde{f}$  stems from  $f_{\text{ejec}} \equiv \tilde{f} \frac{M_T}{R}$  and  $\bar{R} \equiv \frac{1}{2} \sum_{i=1,2} R_i$ . This redefinition of the ejected baryonic mass parameter partly accounts for the compactness of the mass-radius relation of the merging NSs and the associated EoS (supposed to be the same for both NSs).

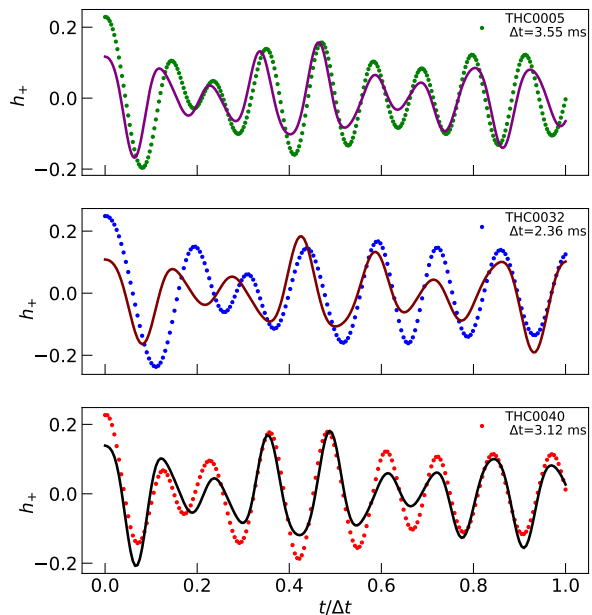


FIG. 2: BNS gravitational waveform from CoRe data base (points) and GW polarizations  $h_+$  (solid lines) as computed from Eq.(11). Fitting parameters appear in Table (I). From top to bottom panel we depict the post-merger time interval  $\Delta_t = 3.55$  ms for THC0005 (green points),  $\Delta_t = 2.36$  ms for THC0032 (blue points) and  $\Delta_t = 3.12$  ms for THC0040 (red points). Time axis is scaled as  $t/\Delta_t$  for each case.  $h_+$  is rescaled by a  $10^{-22}$  factor.

## 3. Setup

Using the CoRe database selected cases and the parameter space described in the section II A 2, we proceed to fit the proposed DO model. To this end, we employ the open-source emcee module in Python [46] which implements the Metropolis-Hastings method as a variant of the Markov Chain Monte Carlo algorithm [46]. Using MCMC we explore the parameter space spanned by the 10-tuple of physical quantities associated with the model, and minimize the distance between CoRe simulation provided main mode  $h^{22}$  and the output of the equations of motion in our model shown in Eq.(10) from which the solutions  $r(t), \theta(t)$  obtained with a Runge-Kutta method are used to construct the GW polarization modes  $h_+(t)$  and  $h_\times(t)$  in the form Eq.(14) and Eq.(15).

The simulation data consist of the early post-merger stage of the GW normalized in the temporal coordinate. This normalization significantly facilitates the search for parameter space; however, it must be taken into account when attempting to recover the values of the frequencies associated with this stage. So setting  $t_{\text{merger}} = 0$  the time

intervals for each of the data sets THC005, THC0032, and THC0040 will be  $\Delta t_{\text{THC005}} = 3.55$  ms,  $\Delta t_{\text{THC0032}} = 2.36$  ms,  $\Delta t_{\text{THC0040}} = 3.12$  ms, respectively. In addition, we place physically informed priors on some parameters from existing phenomenological studies.

For example, for mass values, such as  $m_1$  and  $m_2$ , stricter constraints are applied from the database instance itself, whereas for others, like  $\alpha_2, \beta_n$ , for which expected values are less clear, much broader priors are allowed.

Thus, we first identify a set of 10-tuples that fit the early post-merger window for each THC00XX DM-free simulation. The plot of polarizations with fixed parameters to the vectors of the best fit is shown in Fig. (2). More in detail we specify the best fit (as provided by emcee) and the median value along statistical sigma-deviation  $\langle x \rangle \pm \sigma(x)$  for each fitted parameter. These values are summarized in the Table (I).

#### 4. Effective viscosity

Discussing the viscosity of matter in an extreme environment like this proves to be very challenging due to the assumed hybrid nature, ordinary and dark, of matter under study. For strongly interacting matter it is still poorly understood [47] but it is expected it may impact emitted GW patterns [48] while for DM itself we only have some astrophysical and cosmological hints obtained from phenomenology in large-scale structure, where some works [49] describe that CDM may acquire viscous character from decaying to relativistic particles or scattering ordinary matter. In our setting, we will consider the BNS merging event in a quasi-static phase approximation during which the density in the disk during the time window analyzed remains nearly constant so that we can characterize it by an effective kinetic viscosity value. Most works, in practice, consider an interval with different values of the bulk-viscosity coefficient  $\sim [0.2, 1] \times 10^{30}$  g/cms as in [50]. In that work, authors find that bulk-viscous effects reduce the radiated energy by  $\lesssim 1\%$  in the scenario of small viscosity, and at most by  $\sim 15\%$  in the scenario of large viscosity. In our calculations, we find fitting scenarios with large/small effective hadronic viscosity parameters, see Table (II).

At this point, it is important to note that in our model dissipative forces are described by characteristic  $\alpha_2, \beta_n$  functions where we have made explicit their dependence in linear density. This implies that if we want to compare with microscopic calculations we must first convert them to the well-known dynamic viscosity coefficient. In general, a kinetic viscosity can be defined as  $\alpha = \frac{\mu}{\rho}$  where  $\mu$  is the dynamic viscosity and  $\rho$  is the average volumetric mass density of the merging NS system. In order to

convert quantities we write for our model

$$l_c \rho_{\text{eff}} \alpha_{\text{eff}} = \alpha_2 f_{\text{ejec}} \frac{M_T}{R_d}, \quad (18)$$

where  $R_d$  is the disk radius and  $l_c$  represents a characteristic length of the system, physically motivated by the drifting objects, see below. Thus, if we define the density of the disk as that of a cylinder with a height  $h < R_d$ , we obtain

$$\rho_{\text{eff}} = \frac{f_{\text{ejec}} M_T}{\pi h R_d^2}. \quad (19)$$

From this, it follows that baryon effective kinetic viscosity  $\alpha_{\text{eff}}$  with respect to original viscosity  $\alpha_2$  will be

$$\alpha_{\text{eff}} = \pi \frac{h}{l_c} R_d \alpha_2. \quad (20)$$

Given that we have taken an approximate radius  $R_d \simeq 15.44$  km, we can place bounds on the height of the matter disk as  $2R_S < h < 2R_d$  such that it is smaller than disk diameter and greater than twice the Schwarzschild radius,  $R_S$ , of the associated mass of the nuclei oscillating inside, we fix  $h \sim 15$  km. Thus, we take the characteristic distance of the system such that it is on the order of twice the Schwarzschild radius, which holds for all the cases studied in this article as  $l_c \lesssim 2G\bar{M}/c^2 \sim 9$  km,  $\bar{M} \equiv (m_1 + m_2)/2$ . The conversion can be expressed as  $\mu = \alpha_{\text{eff}} \rho$ . Using the values collected in Table I and based on the above assumptions, we can determine in concordance [51] typical values for the BNS merger data sets, see Table (II).

### III. SPECTRAL PROPERTIES

One interesting property characterizing GW emission in BNS mergers appears to be the quasi-universal nature of their frequency spectrum. More in detail, these frequencies can be determined both during the inspiral phase of two compact objects and following their merger. Additionally, it is worth noting that while the precise positioning of peaks in the frequency spectrum may be influenced by the NS matter EoS, this influence can be readily eliminated to establish relationships between peak frequencies and properties of the progenitor stars that are independent of the EoS [52]. From this, one can conclude that the relationship between the BNS inspiral and post-merger stages would provide an opportunity to investigate the NS structure [41] and BH collapse [53] and environmental effects in which the merger occurs or further distortion of gravitational waveforms showing hints of exotic matter types within the progenitor stars.

One example of the mentioned quasi-universal relations can be found after the careful analysis of GW spectra obtained from simulations [54]. The characteristic frequency, commonly denoted by  $f_{\text{max}}$ , representing the frequency at peak amplitude in the post-merger phase is



Vector	THC0005		THC0032		THC0040	
	Best Fit	$\langle x \rangle \pm \sigma(x)$	Best Fit	$\langle x \rangle \pm \sigma(x)$	Best Fit	$\langle x \rangle \pm \sigma(x)$
$k [M_\odot/ms^2]$	2683.49	2719.58 $\pm$ 54.37	1658.17	1648.53 $\pm$ 25.57	2506.34	2551.38 $\pm$ 54.13
$\alpha_2 [km/ms]$	103.18	111.42 $\pm$ 12.19	2.11	8.22 $\pm$ 8.01	100.30	105.44 $\pm$ 10.68
$\omega_0 [1/ms]$	4.19	4.25 $\pm$ 0.06	4.18	4.12 $\pm$ 1.11	4.24	4.28 $\pm$ 1.93
$r_0 [km]$	2.50	2.59 $\pm$ 0.09	2.94	3.05 $\pm$ 0.19	2.54	2.59 $\pm$ 0.73
$l [km]$	6.75	6.80 $\pm$ 0.16	8.06	8.26 $\pm$ 0.32	7.07	7.10 $\pm$ 1.11
$f [km/M_\odot]$	0.27	0.24 $\pm$ 0.03	0.21	0.20 $\pm$ 0.02	0.33	0.27 $\pm$ 0.07
$m_1 [M_\odot]$	1.44	1.41 $\pm$ 0.03	1.18	1.18 $\pm$ 0.03	1.48	1.43 $\pm$ 0.11
$m_2 [M_\odot]$	1.18	1.21 $\pm$ 0.03	1.42	1.40 $\pm$ 0.03	1.26	1.31 $\pm$ 0.08

TABLE I: The values of the fitted 10-tuple in DM free parameter space fitting selected early post-merger GW waveforms in Fig.(1). The first column (vector) shows the 10-tuple quantities in parameter space along with units. The Best Fit and  $\langle x \rangle \pm \sigma(x)$  columns are obtained using the MCMC method. Details are described in Section II A 3.

DATA	$\alpha_{\text{eff}} [\text{cm}^2/\text{s}]$	$\rho [\text{g}/\text{cm}^3]$	$\mu [\text{g}/\text{cms}]$
THC0005	$2.351 \times 10^{16}$	$0.274 \times 10^{14}$	$0.644 \times 10^{30}$
THC0032	$0.072 \times 10^{16}$	$0.220 \times 10^{14}$	$0.0158 \times 10^{30}$
THC0040	$2.602 \times 10^{16}$	$0.345 \times 10^{14}$	$0.898 \times 10^{30}$

TABLE II: The effective kinetic viscosity ( $\alpha_{\text{eff}}$ ), density ( $\rho$ ) and bulk viscosity ( $\mu$ ) values for the baryonic matter within the BNS merger disk, presented in the cgs system, corresponding to various datasets used in this work.

correlated to the tidal deformability  $\Lambda$  of individual stars as shown in [55]. For this the authors use a set of simulations with  $q \sim 1$  and  $M_T = 2.7M_\odot$ . Remarkably in that work they find  $\log_{10}(\frac{f_{\text{max}}}{\text{Hz}}) = 3.69652 - 0.131743\Lambda^{1/5}$  where  $\Lambda \equiv \frac{2}{3}k_2(\frac{\bar{R}}{\bar{M}})^5$  and  $\bar{R}$  and  $\bar{M}$  the radius and mass of the binary system, respectively.  $k_2$  is the  $l, m = 2, 0$  tidal Love number. The quantities with a bar are defined as averages, i.e.,  $\bar{A} \equiv (A_1 + A_2)/2$ . They also find a weaker correlation of  $f_{\text{max}}$  with compactness  $C$ .

When unequal NS masses are used the relation adopts a slightly different form [1]

$$\log_{10} \left( \frac{f_{\text{max}}}{\text{Hz}} \right) \approx 4.2423 - 0.1546\Lambda^{1/5} - \log_{10} \left( \frac{2\bar{M}}{M_\odot} \right). \quad (21)$$

This equation provides us with a way to relate the characteristic frequency of the GW at peak amplitude with the structure of the NSs involved in the merger. More specifically it involves the universality of  $\bar{M}f_{\text{max}}$ . Recent works point out that the ultimate reason for this could be due to the excitation of asteroseismology modes [56].

What is most intriguing is that relationships like Eq.(21) could enable us to infer the shape of the frequency spectrum during post-merger phases, relying solely on the information available during the inspiral (cold matter) phase. This would open up the possibility of comparing the complex spectrum of the measured GW in early post-merger with what can be inferred from the more tractable inspiral phase. Any discrepancies between two inspiral spectra for similar BNS events could provide valuable insights into the conditions of the envi-

ronment in which the merger occurs, including the potential presence of DM or other interesting astrophysical phenomena.

We now set a distance  $d = 50$  Mpc and analyze the PSD, more precisely taken as  $2\tilde{h}(f)f^{1/2}$  where  $\tilde{h}(f)$  is defined as the Fourier transform  $\tilde{h}(f) \equiv \left| \tilde{h}_+(f) \right|$  and from the  $h_+(t)$  polarization

$$\tilde{h}_+(f) \equiv \int_0^{t_w} h_+(t)e^{-ift} dt \quad (22)$$

where  $t_w$  is the early-postmerger window time  $\Delta t$  that we defined for each signal, see Fig. (2). The transform is taken over this polarization mode due to the approximation to the principal mode  $h_+ \simeq h^{22}$ .

Now we can calculate the logarithm of the spectral density  $\log_{10} \left( 2\tilde{h}(f)f^{1/2} \right) [\text{Hz}^{-1/2} 50\text{Mpc}]$  and study, first, the benchmark results from DM free selected CoRe database simulations and then proceed to see the impact of the (viscous) dark component.

In Fig. (3) we plot our results for the three data sets THC005, THC0032, and THC0040 in the left, center, and right columns, respectively. We depict with a thin red line the full post-merger stage of the data and with thick orange, green, and blue lines the early post-merger interval  $\Delta t$  associated with each dataset utilized. We set  $\beta_2 = 0$  in this panel for all studied cases. The orange line shows the DM free case, while the orange and blue set  $f_\chi = 1\%$  and  $f_\chi = 5\%$  DM mass fraction, respectively. For the upper panel  $\beta_1 = 0.5 \times 10^{16} (\text{cm/s})^2$ , middle  $\beta_1 = 0.25 \times 10^{16} (\text{cm/s})^2$  and lower  $\beta_1 = 0$ . In order to see how feasible a future detection may be we superimpose the sensitivity curves of the Advanced LIGO, ET, NEMO and Cosmic Explorer detectors. We obtain  $f_{\text{max}} = 2.3426, 2.9608$  and  $2.6667$  kHz for THC0005, THC0032, THC0040 cases, respectively. Note that the DM influence related to mass fraction is expected to be small in  $\Lambda$  as already shown in Fig. (5) in our previous work [4]. For our set of EoS the nuclear matter incompressibility  $K \in [242.7, 245.5]$  MeV at saturation density, thus to this respect we are showing cases with a small stiffness spread. We nevertheless see that as shown in [4]



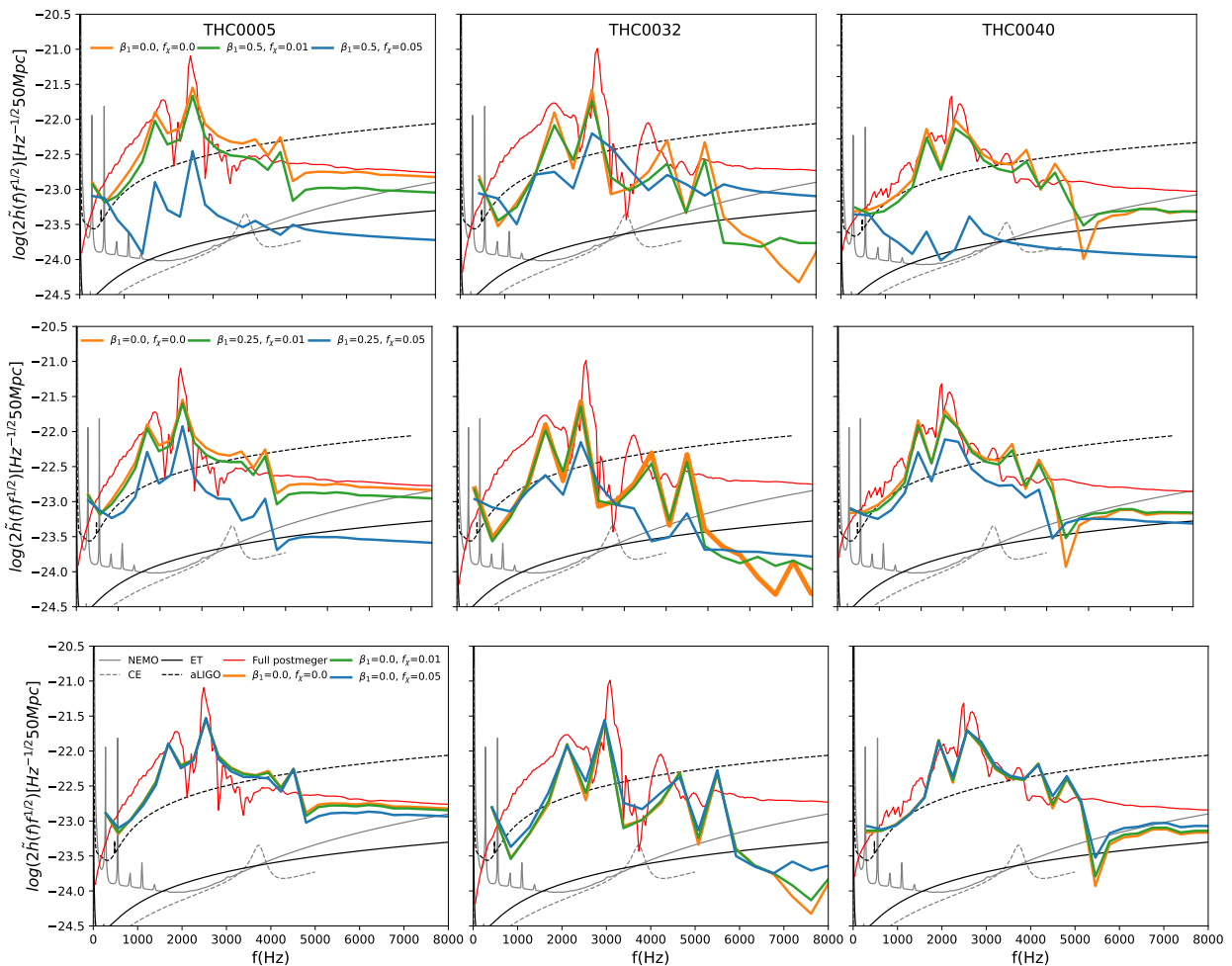


FIG. 3: Panel represents the spectral density  $\sqrt{S_h(f)} = 2\tilde{h}(f)f^{1/2}$  computed for the full post-merger data (thin red line) and for the early post-merger interval after the fitting procedure (thick colored lines) obtained from variation of DM parameters ( $f_\chi, \beta_1$ ) with  $\beta_2 = 0$ .  $\beta_1$  is expressed in  $10^{16}(\text{cm/s})^2$  units. We also plot sensitivity curves of the NEMO, CE, ET and aLIGO detectors (black and grey curves). Data sets THC005, THC0032, and THC0040 appear in the left, center, right columns, respectively. The lower panel shows the case of  $\beta_1 = 0$ . In all cases  $d = 50$  Mpc.

small compactness stars are more sensitive to a  $f_\chi \neq 0$  fraction and thus more likely to show deviations of the DM free  $f_{\text{max}}$  value.

Upon analyzing the frequency spectrum families obtained from our model, it becomes evident how accurately the model replicates the principal peak  $f_{\text{max}}$ , which characterizes the post-merger signal, across the entire temporal interval of the simulated signal. This feature is expected, as this peak is commonly attributed to the inherent quadrupolar oscillation of the system. Furthermore, the model successfully captures a secondary, lower frequency peak,  $f_1$ , at low frequencies associated with a non-linear coupling between the quadrupolar oscillation modes and the quasi-radial modes. It should be noted, in addition, that the primary contributions belong to kHz frequencies, where the peaks appear to originate almost entirely during the early post-merger stage, as illustrated in [1] for the peak at lower frequencies. Similarly, con-

cerning the largest amplitude peak, it has been observed to grow rapidly in the early post-merger stage and then remain almost unchanged throughout the remainder of the post-merger period [57].

In the following, we discuss the obtained results for the PSD. We first consider that the environmental DM causes dissipation in the system that is constant and proportional to linear DM density. This behavior is sometimes referred to in the literature as *Coulomb damping* [58]. In this case, there is only a non-zero  $\beta_n$  i.e.  $\beta_1 \neq 0$  in Section II and we fix  $\beta_2 = 0$ . For decreasing values of  $\beta_1$  characterizing DM behavior we show (left, center and right panels) the PSD for the THC005, THC0032, and THC0040 cases (thick colored lines) considered in Fig. (3). We set  $d = 50$  Mpc. The amplitude of the frequency peaks exhibits more pronounced deviations from the DM-free case ( $f_\chi = \beta_n = 0$ ). This is especially relevant in the right end of the  $f_\chi \in [0.01, 0.05]$  interval. Importantly,

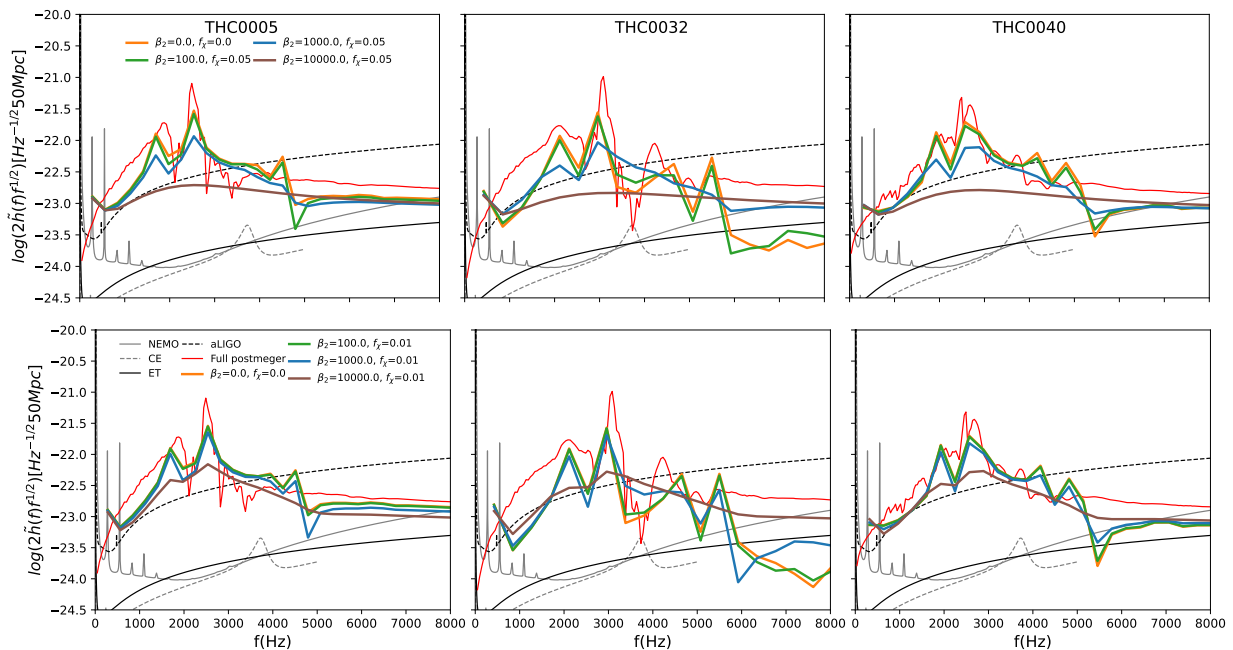


FIG. 4: Panel represents the spectral density  $\sqrt{S_h(f)} = 2\tilde{h}(f)f^{1/2}$  computed for the full post-merger data (thin red line) and for the early post-merger interval after the fitting procedure (thick colored lines) obtained from variation of DM parameters ( $f_\chi, \beta_2$ ) with  $\beta_1 = 0$ . We also plot sensitivity curves of the NEMO, CE, ET and aLIGO detectors (black and grey curves). Data sets THC005, THC0032, and THC0040 appear in the left, center, right columns, respectively. Distance is fixed to  $d = 50$  Mpc.

the decrease in the amplitudes in  $\sqrt{S_h(f)} = 2\tilde{h}(f)f^{1/2}$  from DM dissipation may result in the post-merger region of the event no longer being resolved by the detector at that distance. Consequently, events could be detected at distances where the inspiral phase is well-determined, but not that of the post-merger phase. In other words, detections of BNS mergers in environments containing modest quantities of viscous DM might exhibit GW emission where the typical post-merger early-phase behavior is not discernible, resembling, instead, a rapid decay toward a BH, for example. As shown in the lower panels, when the fraction of DM remains below the fiducial  $\sim 5\%$  threshold and it is assumed a non-viscous behavior, the spectral density curve exhibits only marginal deviations from the DM free pattern. This observation suggests that the introduction of a limited amount of non-viscous matter does not significantly disrupt the expected spectral characteristics.

In Fig.(4) we analyze the so-called *viscous damping* and set  $\beta_1 \equiv 0$  to examine the frequency spectrum for different values of  $\beta_2 \neq 0$ , using the same mass fractions  $f_\chi = 0, 0.01, 0.05$  as in the previous Fig. (3). Following the same logic as in section (II A 4) and setting the values of  $\beta_2 = 0, 10^2, 10^3, 10^4$  (in  $10^8 \text{cm/s}$  units) the resulting viscosity values are presented in the Table (III). Note that the range in  $\beta_2$  values is larger as it corresponds to tiny  $\sim v_r^2$  dependences.

Let us now consider in more detail the two scenarios

for the environmental conditions typical from merging NS [38]. For the cases analyzed we will set DM density somewhat lower than baryonic matter density. In units of nuclear saturation density  $\rho_{\text{sat}} \sim 2 \times 10^{14} \text{g/cm}^3$ , DM density, mass fraction values are displayed in Table (III) along with viscous parameters and its effective conversion to more familiar  $\text{g/cm s}$  units. Thus for  $\rho_{\chi,14} = 0.1, 0.01$  in units of  $10^{14} \text{g/cm}^3$  the conversion dictates also extreme values for  $\mu_\chi \sim [0.1, 100] \times 10^{30} \text{g/cm s}$ .

In this case of viscous damping, the characteristic peaks of the PSD curve disappear. In Fig. (4), it can be observed that for the case with  $f_\chi = 0.05$  and  $\beta_2 = 10^4$  (in  $10^8 \text{cm/s}$  units), the signal vanished entirely, in contrast with the behavior obtained for DM with Coulomb-type damping, where the signal peak amplitude decreases while maintaining its characteristic shape.

In order to discuss the prospects of detectability we proceed to quantify the damping or attenuation in the maximum peak amplitude  $f_{\text{max}}$  in the PSD due to the existence of a DM polluted environment. For this we calculate the effective signal-to-noise ratio (eSNR) as done in [1]. In our case this could be defined as

$$\text{eSNR} \equiv \frac{2\tilde{h}(f_{\text{max}})\sqrt{f_{\text{max}}}}{S_n(f_{\text{max}})} \quad (23)$$

where  $S_n(f_{\text{max}})$  is the value of the detector's sensitivity

THC0005	$\beta_2$ [ $10^8$ cm/s]	$\mu_\chi$ [ $10^{30}$ g/cms]
$f_\chi = 0.01$	$10^2$	0.106
$\rho_{\chi,14} = 0.0463$	$10^3$	1.060
	$10^4$	10.60
$f_\chi = 0.05$	$10^2$	0.528
$\rho_{\chi,14} = 0.232$	$10^3$	5.28
	$10^4$	52.8
THC0032		
$f_\chi = 0.01$	$10^2$	0.158
$\rho_{\chi,14} = 0.0462$	$10^3$	1.580
	$10^4$	15.80
$f_\chi = 0.05$	$10^2$	0.789
$\rho_{\chi,14} = 0.231$	$10^3$	7.890
	$10^4$	78.90
THC0040		
$f_\chi = 0.01$	$10^2$	0.126
$\rho_{\chi,14} = 0.0484$	$10^3$	1.260
	$10^4$	12.60
$f_\chi = 0.05$	$10^2$	0.528
$\rho_{\chi,14} = 0.242$	$10^3$	5.28
	$10^4$	52.8

TABLE III: The table shows the values of DM parameters  $f_\chi$  and  $\beta_2$  used in Fig. (4), along with their reference values for density  $\rho_\chi$  in units of  $10^{14}$  g/cm<sup>3</sup> and viscosity  $\mu_\chi$  in the cgs unit system.

curve at the frequency where maximum peak amplitude of the GW signal appears.

The eSNR, as a function of the DM phase space  $(\beta_1, f_\chi)$ , constitutes a useful and straightforward tool that allows quantifying the influence of DM on the attenuation of peak amplitudes and the rest of the modes. Note that, in principle, this quantity is generally frequency dependent, eSNR( $f$ ). Considering the lower bound given by the sensitivity curve of aLIGO (indicated by the black dashed lines in Fig. (3)), we observe in Fig. (5) the eSNR isocurves dependence on  $(\beta_1, f_\chi)$  for the THC0032 case (bottom) and in more detail the PSD (top) for selected  $\beta_1 = 0.33, 0.37, 0.4, 0.42, 0.5$  in  $10^{16}(\text{cm/s})^2$  units and  $f_\chi = 0.045$  values. Since  $\beta_2$  is so efficient in the damping behaviour we choose for the sake of illustration, instead, the  $\beta_1$  Coulomb damping. For all cases, we assumed GW detections with optimal orientation at 50 Mpc. At this point we remark that the spectral analysis we perform is conducted within a  $\Delta t$  temporal window and consequently, the depicted PSD reflects only the frequencies that influence the signal's power within this interval.

We rely on previous results, which suggest that the main peak is predominantly associated with the early post-merger phase. During this interval, kHz frequencies are more prominent. However, when DM is introduced, the main peak amplitude decreases, reducing the contribution of these frequencies to the signal. From inspection of the eSNR in the bottom panel we see that there is an enhancement, breaking the attenuation tendency, of the peak amplitude for a band (upper right corner). This

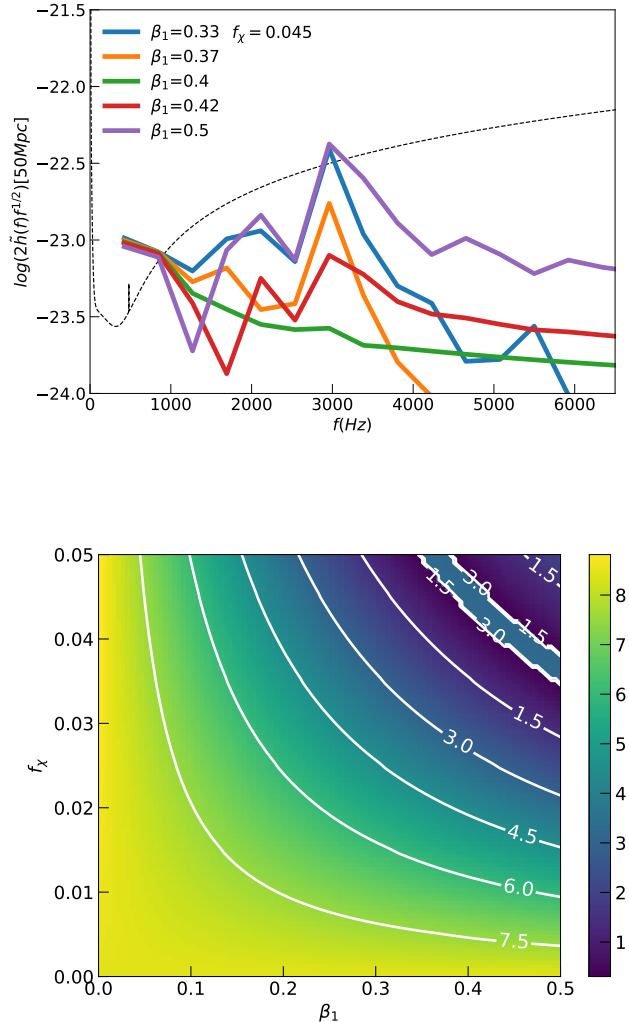


FIG. 5: eSNR as a function of the DM parameters  $(\beta_1, f_\chi)$  for THC0032 (bottom) and PSD (top) with respect to the aLIGO (black dashed line in Fig. 3) for  $\beta_1 = 0.33, 0.37, 0.4, 0.42, 0.5$  in  $10^{16}(\text{cm/s})^2$  units and  $f_\chi = 0.045$  where a non-monotonic eSNR change appears. For all cases, we assumed optimal orientation at  $d=50$  Mpc.

is due to the fact that in this band the peak amplitude shifts towards lower frequency  $\sim 500$  Hz (thus reversing the eSNR ratio decrease) and the original amplitude around  $\sim 3$  kHz falls within aLIGO sensitivity. The detail of this behaviour is illustrated in the top panel where for  $\beta_1 \in [0.33, 0.5]$  and  $f_\chi = 0.045$  the monotony of the main amplitude ratio changes.

#### IV. CONCLUSIONS

We have developed a semi-analytical mechanical Lagrangian model inspired by [1, 17] where an effective elastic potential allows to simulate the dynamics in binary NS mergers in the presence of a DM-polluted environment. This model successfully reproduces the emitted GW signal in a time window for selected early post-merger instances of the CoRe simulation database with no DM. We also analyzed the resulting frequency spectrum and confirmed that the characteristic large amplitude mode,  $f_{\max}$  appearing in the so-called quasi-universal relations, can be recovered in this scenario. By making relatively loose assumptions about the dimensions of the debris disk formed during the early post-merger phase and leveraging the numerical solution results of the model, we obtained values close to those predicted by numerical relativity simulations regarding baryonic density and viscosity.

When the initial (DM free) model is supplemented in a minimal procedure with a non-zero viscous mass fraction of DM in the BNS environment the qualitative behaviour of the GW changes exhibiting a pronounced damping. By analyzing the shape of the frequency spectrum, particularly its characteristic large amplitude peak, we tested the implications of adding up to realistic 5% of matter from the environment. Three fundamental cases were analyzed: matter that does not dissipate the system's energy, and matter that causes dissipation, where we considered two types of dissipation—Coulomb and viscous. For the inviscid matter, we found negligible changes in the PSD up to 5% DM analyzed. For Coulomb/viscous

damping, we found that the amplitude of the main peak decreases appreciably, not resulting shifted from the  $\sim 3$  kHz value except for some DM parameter region. However frequency dependent DM-induced attenuation does not affect low frequency models as much. This is suggesting that matter with this type of behavior could lead to detections where this peak is not resolved by interferometers and could mimic instead a prompt collapse to a more compact object. When considering the effective SNR we find aLIGO yields a lower bound and could detect the possible effects of damping in maximum amplitude mode yielding a non-monotonic tendency for a subset of DM parameters. There is thus a possible interplay among (ordinary) matter effects and those of viscous DM that should not be overlooked. Further work is necessary to investigate these aspects and elucidate the importance of environmental effects and its imprint in waveforms.

#### ACKNOWLEDGEMENTS

We acknowledge useful discussion from D. Radice, A. Perego, I. de Martino, A. de la Cruz-Dombriz, R. Della Monica and P. Char. We also acknowledge support from Spanish Ministry of Science PID2022-137887NB-10 and RED2022-134411-T projects and European Union's HORIZON MSCA-2022-PF-01-01, project ProMatExNS. D. Suarez-Fontanella gratefully acknowledges the financial support provided by the Banco Santander International Doctoral Scholarship. D. Barba-González acknowledges support from a Ph.D. Fellowship funded by Consejería de Educación de la Junta de Castilla y León and European Social Fund. We acknowledge use of Spanish RES resources.

- 
- [1] K. Takami, L. Rezzolla, and L. Baiotti, *Phys. Rev. D* **91**, 064001 (2015).
  - [2] A. Arbey and F. Mahmoudi, *Prog. Part. Nucl. Phys.* **119**, 103865 (2021), arXiv:2104.11488 [hep-ph].
  - [3] D. J. E. Marsh, D. Ellis, and V. M. Mehta, *Dark Matter: Evidence, Theory, and Constraints* (Princeton University Press, 2024).
  - [4] M. Mariani, C. Albertus, M. d. R. Alessandroni, M. G. Orsaria, M. Á. Pérez-García, and I. F. Ranea-Sandoval, *MNRAS* **527**, 6795 (2024), arXiv:2311.14004 [astro-ph.HE].
  - [5] D. Rafiei Karkevandi, M. Shahrabaf, S. Shakeri, and S. Typel, *Particles* **7**, 201 (2024), arXiv:2402.18696 [astro-ph.HE].
  - [6] E. Oks, *New Astronomy Reviews* **93**, 101632 (2021).
  - [7] F. Zwicky, *Helvetica Physica Acta*, Vol. 6, p. 110-127 **6**, 110 (1933).
  - [8] G. Bertone, D. Croon, M. Amin, K. K. Boddy, B. Kavanagh, K. J. Mack, P. Natarajan, T. Opferkuch, K. Schutz, V. Takhistov, C. Weniger, and T.-T. Yu, *SciPost Physics Core* **3**, 10.21468/scipostphyscore.3.2.007 (2020).
  - [9] B. P. Abbott, R. Abbott, T. D. Abbott, M. R. Abernathy, F. Acernese, K. Ackley, C. Adams, T. Adams, P. Addesso, R. X. Adhikari, V. B. Adya, C. Affeldt, M. Agathos, K. Agatsuma, N. Aggarwal, O. D. Aguiar, L. Aiello, A. Ain, P. Ajith, B. Allen, A. W. Allocca, T. Denker, T. Dent, H. Dereli, V. Dergachev, R. T. DeRosa, R. De Rosa, R. DeSalvo, S. Dhurandhar, M. C. Díaz, L. Di Fiore, M. Di Giovanni, A. Di Lieto, S. Di Pace, I. Di Palma, A. Di Virgilio, G. Dojcinoski, V. Dolique, F. Donovan, K. L. Dooley, S. Doravari, R. Douglas, T. P. Downes, M. Drago, R. W. P. Drever, J. C. Driggers, Z. Du, D. Ducrot, M., B. Hughey, S. Husa, S. H. Huttner, T. Huynh-Dinh, A. Idrisy, J.-P. Indik, M. Zevin, F. Zhang, L. Zhang, M. Zhang, Y. Zhang, C. Zhao, M. Zhou, Z. Zhou, X. J. Zhu, M. E. Zucker, S. E. Zuraw, and J. Zweizig (LIGO Scientific Collaboration and Virgo Collaboration), *Phys. Rev. Lett.* **116**, 131103 (2016).
  - [10] R. Abbott, T. D. Abbott, F. Acernese, K. Ackley, C. Adams, N. Adhikari, R. X. Adhikari, V. B. Adya, Y. Affeldt, C. anang, C. Zhao, G. Zhao, Y. Zhao, Y. Zhao, Y. Zheng, R. Zhou, Z. Zhou, X. J. Zhu, Z.-H.

- Zhu, A. B. Zimmerman, Y. Zlochower, M. E. Zucker, and J. Zweizig (LIGO Scientific Collaboration, Virgo Collaboration, and KAGRA Collaboration), *Phys. Rev. X* **13**, 011048 (2023).
- [11] A. H. Nitz, S. Kumar, Y.-F. Wang, S. Kastha, S. Wu, M. Schäfer, R. Dhurkunde, and C. D. Capano, *The Astrophysical Journal* **946**, 59 (2023).
- [12] M. Evans, A. Corsi, C. Afle, A. Ananyeva, K. G. Arun, S. Ballmer, A. Bandopadhyay, L. Barsotti, M. Baryakhtar, E. Berger, E. Berti, S. Biscoveanu, S. Borhanian, F. Broekgaarden, D. A. Brown, C. Cahillane, L. Campbell, H.-Y. Chen, K. J. Daniel, A. Dhani, J. C. Driggers, A. Effler, R. Eisenstein, S. Fairhurst, J. Feicht, P. Fritschel, P. Fulda, I. Gupta, E. D. Hall, G. Hammond, O. A. Hannuksela, H. Hansen, C.-J. Haster, K. Kacanja, B. Kamai, R. Kashyap, J. S. Key, S. Khadkikar, A. Kontos, K. Kuns, M. Landry, P. Landry, B. Lantz, T. G. F. Li, G. Lovelace, V. Mandic, G. L. Mansell, D. Martynov, L. McCuller, A. L. Miller, A. H. Nitz, B. J. Owen, C. Palomba, J. Read, H. Phurailatpam, S. Reddy, J. Richardson, J. Rollins, J. D. Romano, B. S. Sathyaprakash, R. Schofield, D. H. Shoemaker, D. Sigg, D. Singh, B. Slagmolen, P. Sledge, J. Smith, M. Soares-Santos, A. Strunk, L. Sun, D. Tanner, L. A. C. van Son, S. Vitale, B. Willke, H. Yamamoto, and M. Zucker, *Cosmic explorer: A submission to the nsf mpac nggw subcommittee* (2023), arXiv:2306.13745 [astro-ph.IM].
- [13] M. Branchesi, M. Maggiore, D. Alonso, C. Badger, B. Banerjee, F. Beirnaert, E. Belgacem, S. Bhagwat, G. Boileau, S. Borhanian, D. D. Brown, M. Leong Chan, G. Cusin, S. L. Danilishin, J. Degallaix, V. De Luca, A. Dhani, T. Dietrich, U. Dupletsa, S. Foffa, G. Franciolini, A. Freise, G. Gemme, B. Goncharov, A. Ghosh, F. Gulminelli, I. Gupta, P. Kumar Gupta, J. Harms, N. Hazra, S. Hild, T. Hinderer, I. Siong Heng, F. Iacovelli, J. Janquart, K. Janssens, A. C. Jenkins, C. Kalaghatgi, X. Korovesi, T. G. Li, Y. Li, E. Lofredo, E. Maggio, M. Mancarella, M. Mapelli, K. Martinovic, A. Maselli, P. Meyers, A. L. Miller, C. Mondal, N. Muttoni, H. Narola, M. Oertel, G. Oganessian, C. Pacilio, C. Palomba, P. Pani, A. Pasqualetti, A. Perego, C. Péroigois, M. Pieroni, O. J. Piccinni, A. Puecher, P. Puppo, A. Ricciardone, A. Riotto, S. Ronchini, M. Sakellariadou, A. Samajdar, F. Santoliuqido, B. Sathyaprakash, J. Steinlechner, S. Steinlechner, A. Utina, C. Van Den Broeck, and T. Zhang, *Journal of Cosmology and Astroparticle Physics* **2023** (07), 068.
- [14] K. Ackley, V. B. Adya, P. Agrawal, P. Altin, G. Ashton, M. Bailes, E. Baltinas, A. Barbuio, D. Beniwal, C. Blair, D. Blair, G. N. Bolingbroke, V. Bossilkov, S. Shachar Boubilil, D. D. Brown, B. J. Burridge, J. Calderon Bustillo, J. Cameron, H. Tuong Cao, J. B. Carlin, S. Chang, P. Charlton, C. Chatterjee, D. Chattopadhyay, X. Chen, J. Chi, J. Chow, Q. Chu, A. Ciobanu, T. Clarke, P. Clearwater, J. Cooke, D. A. Coward, H. Crisp, R. J. Dattatri, A. T. Deller, D. A. Dobie, L. Dunn, P. J. Easter, J. Eichholz, R. Evans, C. Flynn, G. Foran, P. Forsyth, Y. Gai, S. Galaudage, D. K. Galloway, B. Gendre, B. Goncharov, S. Goode, D. Gozzard, B. Grace, A. W. Graham, A. Heger, F. Hernandez Vivanco, R. Hirai, N. A. Holland, Z. J. Holmes, E. Howard, E. Howell, G. Howitt, M. T. Hübner, J. Hurley, C. Ingram, V. Jaberian Hamedan, K. Jenner, L. Ju, D. P. Kapasi, T. Kaur, N. Kijbunchoo, M. Kovalam, R. Kumar Choudhary, P. D. Lasky, M. Y. M. Lau, J. Leung, J. Liu, K. Loh, A. Mailvagan, I. Mandel, J. J. McCann, D. E. McClelland, K. McKenzie, D. McManus, T. McRae, A. Melatos, P. Meyers, H. Middleton, M. T. Miles, M. Millhouse, Y. Lun Mong, B. Mueller, J. Munch, J. Musiov, S. Muusse, R. S. Nathan, Y. Naveh, C. Neijssel, B. Neil, S. W. S. Ng, V. Oloworaran, D. J. Ottaway, M. Page, J. Pan, M. Pathak, E. Payne, J. Powell, J. Pritchard, E. Puckridge, A. Raidani, V. Rallabhandi, D. Reardon, J. A. Riley, L. Roberts, I. M. Romero-Shaw, T. J. Roocke, G. Rowell, N. Sahu, N. Sarin, L. Sarre, H. Sattari, M. Schiowski, S. M. Scott, R. Sengar, D. Shaddock, R. Shannon, J. SHL, P. Sibley, B. J. J. Slagmolen, T. Slaven-Blair, R. J. E. Smith, J. Spollard, L. Steed, L. Strang, H. Sun, A. Sunderland, S. Suvorova, C. Talbot, E. Thrane, D. Töyrä, P. Trahanas, A. Vajpeyi, J. V. van Heijningen, A. F. Vargas, P. J. Veitch, A. Vigna-Gomez, A. Wade, K. Walker, Z. Wang, R. L. Ward, K. Ward, S. Webb, L. Wen, K. Wette, R. Wilcox, J. Winterflood, C. Wolf, B. Wu, M. Jet Yap, Z. You, H. Yu, J. Zhang, J. Zhang, C. Zhao, and X. Zhu, *Publications of the Astronomical Society of Australia* **37**, 10.1017/pasa.2020.39 (2020).
- [15] P. Amaro-Seoane, H. Audley, S. Babak, J. Baker, E. Barausse, P. Bender, E. Berti, P. Binetruy, M. Born, D. Bortoluzzi, J. Camp, C. Caprini, V. Cardoso, M. Colpi, J. Conklin, N. Cornish, C. Cutler, K. Danzmann, R. Dolesi, L. Ferraioli, V. Ferroni, E. Fitzsimons, J. Gair, L. G. Bote, D. Giardini, F. Gibert, C. Grigani, H. Halloin, G. Heinzel, T. Hertog, M. Hewitson, K. Holley-Bockelmann, D. Hollington, M. Hueller, H. Inchauspe, P. Jetzer, N. Karnesis, C. Killow, A. Klein, B. Klipstein, N. Korsakova, S. L. Larson, J. Livas, I. Lloro, N. Man, D. Mance, J. Martino, I. Mateos, K. McKenzie, S. T. McWilliams, C. Miller, G. Mueller, G. Nardini, G. Nelemans, M. Nofrarias, A. Petiteau, P. Pivato, E. Plagnol, E. Porter, J. Reiche, D. Robertson, N. Robertson, E. Rossi, G. Russano, B. Schutz, A. Sesana, D. Shoemaker, J. Slutsky, C. F. Sopuerta, T. Sumner, N. Tamanini, I. Thorpe, M. Troebs, M. Vallisneri, A. Vecchio, D. Vetrugno, S. Vitale, M. Volonteri, G. Wanner, H. Ward, P. Wass, W. Weber, J. Ziemer, and P. Zweifel, *Laser interferometer space antenna* (2017), arXiv:1702.00786 [astro-ph.IM].
- [16] T. L. S. Collaboration, the Virgo Collaboration, and the KAGRA Collaboration, *Observation of gravitational waves from the coalescence of a 2.5–4.5  $m_{\odot}$  compact object and a neutron star* (2024), arXiv:2404.04248 [astro-ph.HE].
- [17] J. Ellis, A. Hektor, G. Hütsi, K. Kannike, L. Marzola, M. Raidal, and V. Vaskonen, *Physics Letters B* **781**, 607 (2018).
- [18] G. Ashton, M. Hübner, P. D. Lasky, C. Talbot, K. Ackley, S. Biscoveanu, Q. Chu, A. Divakarla, P. J. Easter, B. Goncharov, F. H. Vivanco, J. Harms, M. E. Lower, G. D. Meadors, D. Melchor, E. Payne, M. D. Pitkin, J. Powell, N. Sarin, R. J. E. Smith, and E. Thrane, *The Astrophysical Journal Supplement Series* **241**, 27 (2019).
- [19] R. Garani, N. Raj, and J. Reynoso-Cordova, *J. Cosmology Astropart. Phys.* **2023**, 038 (2023), arXiv:2303.18009 [astro-ph.HE].
- [20] D. H. Weinberg, J. S. Bullock, F. Governato, R. Kuzio de Naray, and A. H. G. Peter, *Proceedings of the National*

- Academy of Science **112**, 12249 (2015), arXiv:1306.0913 [astro-ph.CO].
- [21] M. R. Mosbech, A. C. Jenkins, S. Bose, C. Boehm, M. Sakellariadou, and Y. Y. Y. Wong, *Phys. Rev. D* **108**, 043512 (2023).
- [22] B. Fornal, K. Garcia, and E. Pierre, *Phys. Rev. D* **108**, 055022 (2023).
- [23] R. Samanta and F. R. Urban, *Journal of Cosmology and Astroparticle Physics* **2022** (06), 017.
- [24] B. Fornal, K. Garcia, and E. Pierre, *Phys. Rev. D* **108**, 055022 (2023).
- [25] S. Banerjee, S. Bera, and D. F. Mota, *Journal of Cosmology and Astroparticle Physics* **2023** (03), 041.
- [26] A. Ghoshal and A. Strumia, Probing the dark matter density with gravitational waves from super-massive binary black holes (2023), arXiv:2306.17158 [astro-ph.CO].
- [27] A. K. Mishra, *The European Physical Journal C* **82**, 1060 (2022).
- [28] B.-Q. Lu, D. Huang, Y.-L. Wu, and Y.-F. Zhou, Damping of gravitational waves in a viscous universe and its implication for dark matter self-interactions (2018), arXiv:1803.11397 [astro-ph.HE].
- [29] I. Brevik and S. Nojiri, *International Journal of Modern Physics D* **28**, 1950133 (2019), <https://doi.org/10.1142/S0218271819501335>.
- [30] T. Dietrich, D. Radice, S. Bernuzzi, F. Zappa, A. Perego, B. Brügmann, S. V. Chaurasia, R. Dudi, W. Tichy, and M. Ujevic, *Classical and Quantum Gravity* **35**, 24LT01 (2018).
- [31] D. Radice, S. Bernuzzi, and A. Perego, *Annual Review of Nuclear and Particle Science* **70**, 95 (2020).
- [32] N. F. Bell, G. Busoni, S. Robles, and M. Virgato, *Journal of Cosmology and Astroparticle Physics* **2024** (04), 006.
- [33] A. Herrero, M. A. Pérez-García, J. Silk, and C. Albertus, *Phys. Rev. D* **100**, 103019 (2019).
- [34] S. Banik, M. Hempel, and D. Bandyopadhyay, *ApJS* **214**, 22 (2014), arXiv:1404.6173 [astro-ph.HE].
- [35] A. W. Steiner, M. Hempel, and T. Fischer, *The Astrophysical Journal* **774**, 17 (2013).
- [36] S. Typel, G. Röpke, T. Klähn, D. Blaschke, and H. H. Wolter, *Phys. Rev. C* **81**, 015803 (2010), arXiv:0908.2344 [nucl-th].
- [37] A. Perego, S. Bernuzzi, and D. Radice, *European Physical Journal A* **55**, 10.1140/epja/i2019-12810-7 (2019), publisher Copyright: © 2019, Società Italiana di Fisica and Springer-Verlag GmbH Germany, part of Springer Nature.
- [38] F. Foucart, M. D. Duez, L. E. Kidder, H. P. Pfeiffer, and M. A. Scheel, *Phys. Rev. D* **110**, 024003 (2024).
- [39] F. Prada, R. Content, A. Goobar, L. Izzo, E. Pérez, A. Agnello, C. del Burgo, V. Dhillon, J. M. Diego, L. Galbany, J. García-Rojas, D. Jones, J. Lawrence, E. Martín, E. Mediavilla, M. Ángeles Pérez García, J. S. Almeida, J. A. A. Pulido, A. R. López-Sánchez, S. Arribas, F. J. Carrera, A. Corral, I. Domínguez, S. Mateos, S. M. Nuñez, E. Villaver, M. R. Z. Osorio, C. Albertus, F. A. Battaia, D. Barrado, V. J. S. Bejar, H. M. J. Boffin, H. Bouy, A. Burgasser, C. Esteban, N. Lodieu, M. M. Calderón, A. P. Garrido, P. R. Gil, A. S. Carracedo, M. S. García, E. Solano, M. A. P. Torres, and R. Wesson, White paper on maat@gtc (2020), arXiv:2007.01603 [astro-ph.IM].
- [40] M. Hanauske and L. R. Weih, *Astronomische Nachrichten* **342**, 788 (2021), <https://onlinelibrary.wiley.com/doi/pdf/10.1002/asna.202113994>.
- [41] M. Bezares, D. Viganò, and C. Palenzuela, *Phys. Rev. D* **100**, 044049 (2019).
- [42] K. Glampedakis and L. Gualtieri, Gravitational waves from single neutron stars: An advanced detector era survey, in *Astrophysics and Space Science Library* (Springer International Publishing, 2018) p. 673–736.
- [43] S. Dall’Osso, L. Stella, and C. Palomba, *Monthly Notices of the Royal Astronomical Society* **480**, 1353–1362 (2018).
- [44] K. S. Thorne, C. W. Misner, and J. A. Wheeler, *Gravitation* (Freeman San Francisco, CA, 2000).
- [45] D. Radice and L. Rezzolla, *A&A* **547**, A26 (2012), arXiv:1206.6502 [astro-ph.IM].
- [46] D. Foreman-Mackey, D. W. Hogg, D. Lang, and J. Goodman, *Publications of the Astronomical Society of the Pacific* **125**, 306–312 (2013).
- [47] M. Alford, A. Harutyunyan, and A. Sedrakian, *Particles* **5**, 361–376 (2022).
- [48] M. G. Alford, L. Bovard, M. Hanauske, L. Rezzolla, and K. Schwenzer, *Physical Review Letters* **120**, 10.1103/physrevlett.120.041101 (2018).
- [49] S. Anand, P. Chaulal, A. Mazumdar, S. Mohanty, and P. Parashari, *Journal of Cosmology and Astroparticle Physics* **2018** (05), 031–031.
- [50] M. Chabanov and L. Rezzolla, Impact of bulk viscosity on the post-merger gravitational-wave signal from merging neutron stars (2023), arXiv:2307.10464 [gr-qc].
- [51] M. Chabanov and L. Rezzolla, arXiv e-prints , arXiv:2307.10464 (2023), arXiv:2307.10464 [gr-qc].
- [52] L. Baiotti and L. Rezzolla, *Reports on Progress in Physics* **80**, 096901 (2017).
- [53] M. Emma, F. Schianchi, F. Pannarale, V. Sagun, and T. Dietrich, Numerical simulations of dark matter admixed neutron star binaries (2022), arXiv:2206.10887 [gr-qc].
- [54] S. Bernuzzi, A. Nagar, S. Balmelli, T. Dietrich, and M. Ujevic, *Physical Review Letters* **112**, 10.1103/physrevlett.112.201101 (2014).
- [55] J. S. Read, L. Baiotti, J. D. E. Creighton, J. L. Friedman, B. Giacomazzo, K. Kyutoku, C. Markakis, L. Rezzolla, M. Shibata, and K. Taniguchi, *Phys. Rev. D* **88**, 044042 (2013).
- [56] F. Gittins and N. Andersson, Neutron-star seismology with realistic, finite-temperature nuclear matter (2024), arXiv:2406.05177 [gr-qc].
- [57] T. Soutanis, A. Bauswein, and N. Stergioulas, *Physical Review D* **105**, 043020 (2022).
- [58] T. H. Fay, *International Journal of Mathematical Education in Science and Technology* **43**, 923 (2012).